CrossMark

Effect of Stress on Corrosion at Crack Tip on Pipeline Steel in a Near-Neutral pH Solution

Yao Yang and Y. Frank Cheng

In this work, the local corrosion at crack tip on an API 5L X46 pipeline steel specimens was investigated under various applied loads in a near-neutral pH solution. Electrochemical measurements, including potentiodynamic polarization and electrochemical impedance spectroscopy, combined with micro-electrochemical technique and surface characterization, were conducted to investigate the effect of stress on local anodic solution of the steel at the crack tip. The stress corrosion cracking of the steel was dominated by an anodic dissolution mechanism, while the effect of hydrogen was negligible. The applied load (stress) increased the corrosion rate at the crack tip, contributing to crack propagation. The deposit of corrosion products at the crack tip could protect somewhat from further corrosion. At sufficiently large applied loads such as 740 N in the work, it was possible to generate separated cathode and anode, further accelerating the crack growth.

1. Introduction

Pipelines have been used as an effective and efficient means for transportation of oil and gas from production sites to refineries and markets. Generally, the pipelines are protected from external corrosion by both coatings and cathodic protection (CP). In reality, the coating can be damaged during transportation and construction of the pipeline. Various failure modes such as disbondment can occur on the coating during service. When the CP becomes shielded from reaching the pipe steel by the coating, corrosion and stress corrosion cracking (SCC) can occur on the pipeline (Ref 1). In the mid-1980s, Canadian pipelines suffered from extensive SCC, where a near-neutral pH environment was generated under disbonded coating (Ref 2). The aqueous environment contains mainly diluted bicarbonate solution, with a pH range between 6.5 and 7.5 due to the shielded CP current from reaching the trapped solution (Ref 1).

The near-neutral pH SCC has been studied on a wide variety of pipeline steels, including API (American Petroleum Institute) 5L X52, X65, X70, X80 and X100 steels (Ref 3-7). It is generally accepted that carbon steel pipelines suffer from SCC in near-neutral pH environments by both anodic dissolution and the hydrogen involvement (Ref 8, 9). For example, Cheng group has investigated the stress-enhanced corrosion at crack tip on pipeline steels (Ref 10, 11), and the effect of hydrogen, including its adsorption and permeation at the crack tip, on increased corrosion and crack propagation (Ref 9, 12). Moreover, researchers have investigated local corrosion and electrochemistry at pits, crevices and cracks (Ref 13, 14), where unique corrosion feature exists compared to that occurring outside the local areas.

In addition to the high grades of pipe steel, low-grade steels, such as API 5L X42 and X46 steels, were also found to experience SCC in the field (Ref 15). Pipelines made of these steels have been in service for 50 years and above. It is expected that their metallurgical features and mechanical properties, which are different from those of high grades of steel, would affect pipeline corrosion and SCC in a way that is unique from the high grades of pipe steel.

In this work, the susceptibility of low-grade API 5L X46 pipeline steel to near-neutral pH SCC was studied by tensile testing, electrochemical and micro-electrochemical measurements and surface analysis technique. The steel corrosion at the crack tip was investigated by potentiodynamic polarization and electrochemical impedance spectroscopy (EIS) measurements, as well as scanning vibrated electrode technique (SVET). The microstructure and surface morphology of the steel specimen were characterized by optical microscopy and scanning electronic microscopy (SEM). The mechanism of the near-neutral pH SCC of X46 steel was discussed.

2. Experimental

2.1 Specimen and Solution

Specimens used in this work were made of a X46 steel pipe, with the chemical composition (wt.%): C 0.24, Mn 1.20, Si 0.26, P 0.02, S 0.022, Ni 0.02, Cr 0.04, Cu 0.02, V 0.05 and Fe balance. Both tensile testing and compact toughness (CT) specimens were machined with the dimension shown in Fig. 1. The CT specimens were pre-fatigued in air according to ASTM 647-15 standard to produce a pre-crack at the root of the notch (Ref 16), where the applied force was 700 N, the number of loading cycles was 50,000 cycles, and the total loading time was nearly 14 h. Prior to testing, the surface of the specimens was ground sequentially to 1200 grit emery paper and then rinsed with deionized water and acetone.

Yao Yang and **Y. Frank Cheng**, Departmental of Mechanical and Manufacturing Engineering, University of Calgary, Calgary, AB T2N 1N4, Canada. Contact e-mail: fcheng@ucalgary.ca.
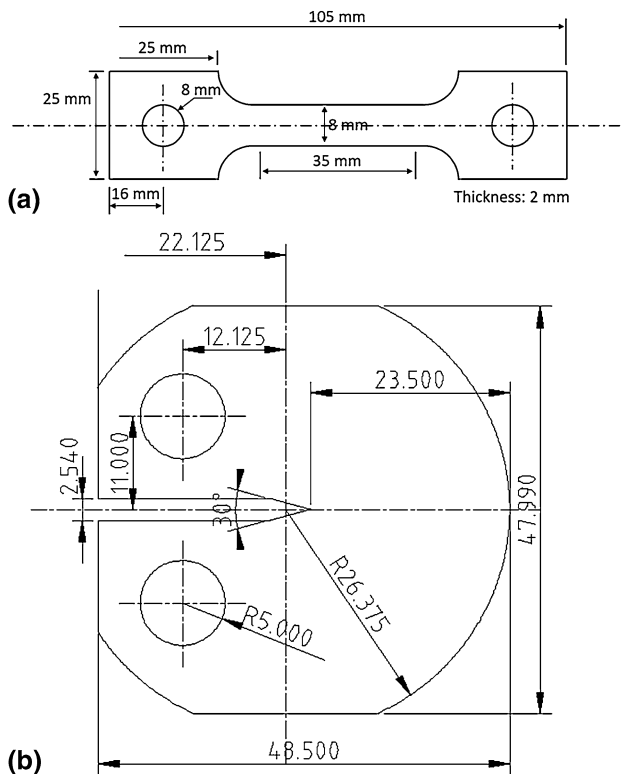
Fig. 1 Schematic diagram of (a) tensile testing specimen and (b) pre-cracked compact toughness specimen with a thickness of 2 mm

For electrochemical measurements, coupons were cut from the steel pipe, with a dimension of 1 cm × 1 cm. The coupons were soldered with a copper wire and embedded into LECO epoxy and cured for 24 h. The exposed surface was ground sequentially to 1200 grit emery paper and cleaned by deionized water and acetone.

A solution named NS4 solution was used in this work to simulate the near-neutral pH electrolyte trapped under disbonded polyethylene coating on pipelines (Ref 17). The chemical composition (g/L) of the solution was $NaHCO_3$ 0.483, KCl 0.122, $CaCl_2 \cdot 2H_2O$ 0.181 and $MgSO_4 \cdot 7H_2O$ 0.131. The solution was made from analytic grade reagents and deionized water. Prior to testing, 5% CO_2 (balanced with N_2) was purged into the solution for 1 h to achieve a pH value between 6.5 and 7. A continuous gas flow at a rate of 20 mL/min was maintained during the test.

All the tests were conducted at ambient temperature, approximately 22 °C.

2.2 Tensile Testing

The engineering stress-strain curve of X46 steel was measured in air on the tensile testing specimen through a Bose Electroforce dynamic materials test system. The test followed the ASTM standard (Ref 18), and the strain rate was set as 3×10^{-4} s^{-1}. To ensure the reproducibility of testing results, each test was performed three times.

2.3 Electrochemical Measurements

The experimental setup for electrochemical measurements at the crack tip is shown in Fig. 2, which contained a home-made three-electrode testing cell and a metal frame with a com-

pressed spring used to apply tensile loads on the specimen. The steel at the crack tip was served as working electrode with an area of 1.5 mm × 1.5 mm and a saturated calomel electrode (SCE) as reference electrode and a graphite rod as counter electrode. The cell contained NS4 solution with 5% CO_2/N_2 gas purging during test. A Gamry Reference 600 electrochemical workstation was used for electrochemical measurements.

After 1 h of immersion of the steel specimen in the solution, the open-circuit potential reached a relatively steady state. The EIS was then measured under a potential disturbance of ±10 mV and within a frequency range of 10^5-10^{-2} Hz. After the EIS measurements, the potentiodynamic polarization curve was measured from cathodic to anodic directions, with a potential scan rate of 0.1 mV/s (Ref 19).

2.4 SVET Measurements

A PAR Model 370 scanning electrochemical workstation was used to measure the localized current density at the crack tip of the specimen by SVET. Similar to the setup in Fig. 2, a microprobe was positioned above the pre-cracked specimen, which was under various tensile loads applied through the compressed spring. The load was calculated by the elastic coefficient and deformation of the spring. The scanning area for SVET measurements was 1.5 mm × 1.5 mm.

During SVET measurements, the microprobe with a 10-μm tip was set above the surface of the specimen. The distance between the probe tip and the specimen was 100 μm. The microprobe vibrated in a direction perpendicular to the specimen surface at a frequency of 80 Hz and a magnitude of 30 μm. The difference of potentials between the vibrating peak and the valley, ΔE, was measured by an electrometer. The conductivity of the NS4 solution was measured by a conductivity meter. The resistance of the solution between the vibrating peak and valley, R, is determined by $R = d/k$, where d is the vibrating amplitude of the microprobe and k is the conductivity of the solution. The localized current density can be calculated by $I = \Delta E/R$, where a flat SVET current density map indicates a uniform corrosion activity of the specimen, while a fluctuating one indicates a non-uniform corrosion activity.

3. Results

3.1 Metallographic Microstructure of X46 Steel

Figure 3 shows the optical and SEM views of the microstructure of X46 steel. The main components of the microstructure of the steel contain ferrite and pearlite, as labeled.

3.2 Stress-Strain Curves of X46 Steel in Air and in NS4 Solution

Figure 4 shows the stress-strain curves of X46 steel in air and after 3 days of immersion in NS4 solution, respectively. The mechanical properties, including yielding strength and tensile strength, and elongation and reduction-in-area of the specimen, as well as the ductility loss factors are shown in Table 1. It is seen that both the elongation and reduction-in-area reduce after soaking in NS4 solution. The results may indicate that the environmental exposure of the steel specimen may
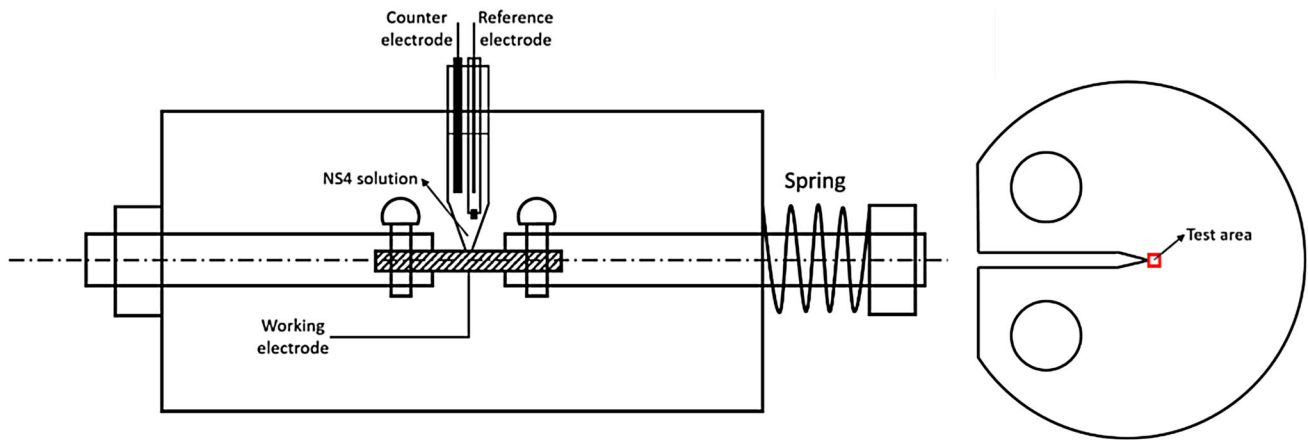
Fig. 2 Schematic diagram of the experimental setup for electrochemical measurements at the crack tip of the steel specimen
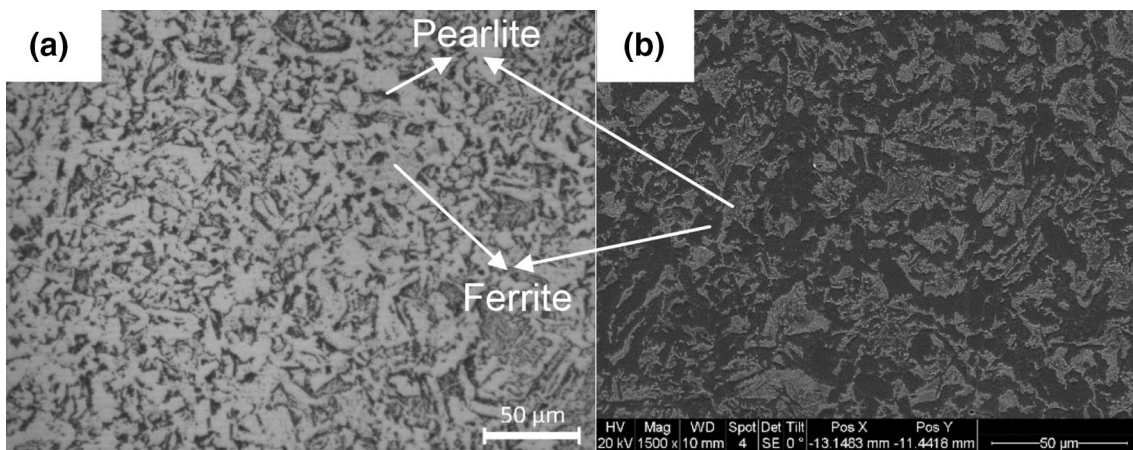

Fig. 3 Microstructure of X46 pipeline steel (a) optical image, (b) SEM image
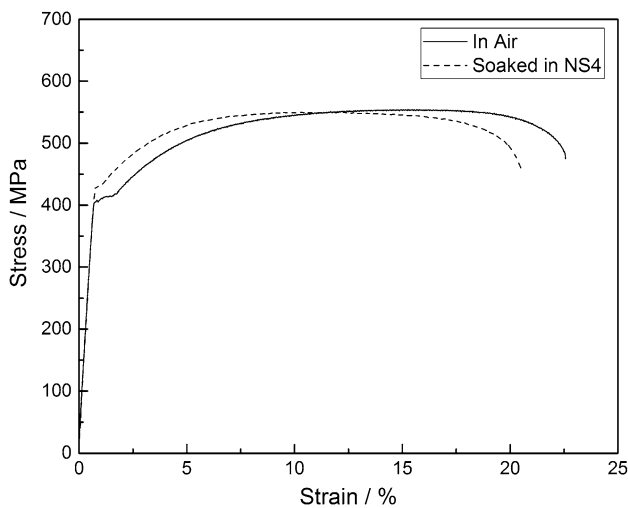

Fig. 4 Stress-strain curves of X46 steel measured in air and after 3 days of soaking in NS4 solution, respectively

decrease its ductility. Furthermore, the ductility loss factors as calculated show that the reduction-in-area is more sensitive to indicate the changed ductility of X46 steel when soaking in NS4 solution compared to that in air.

Table 1 Mechanical properties of X46 steel measured in air and after 3 days of soaking in NS4 solution and the ductility loss factors

	In air	In NS4 solution	Ductility loss factor, %
Yielding strength (MPa)	410	426	/
Tensile strength (MPa)	552	550	0.4
Elongation (%)	21.7	19.7	9.2
Reduction-in-area (%)	47.6	38.6	18.9

3.3 EIS and Polarization Measurements at the Crack Tip in NS4 Solution

Figure 5 shows the Nyquist diagrams and Bode plots measured at the crack tip and on a macroscopic steel specimen under various applied loads in NS4 solution, respectively. The macroscopic steel electrode is used to compare the EIS behavior in the absence of applied load. It is seen that all impedance plots are featured with a depressed semicircle in the high frequency range and an inductive loop in the low frequency range. With the increase in the applied load, the size of the semicircle decreases. The macroscopic electrode which is not under loading is associated with the largest semicircle in Fig. 5(a).
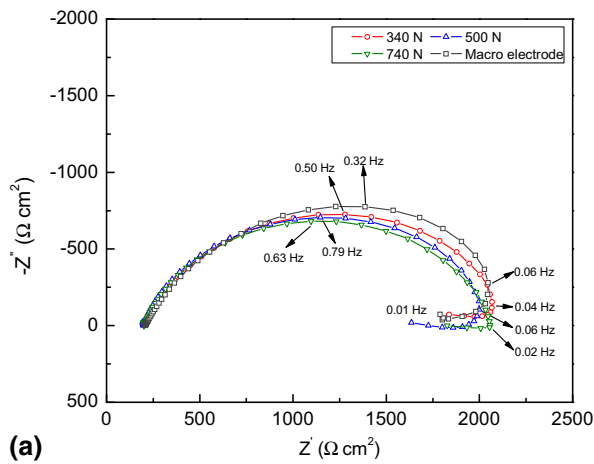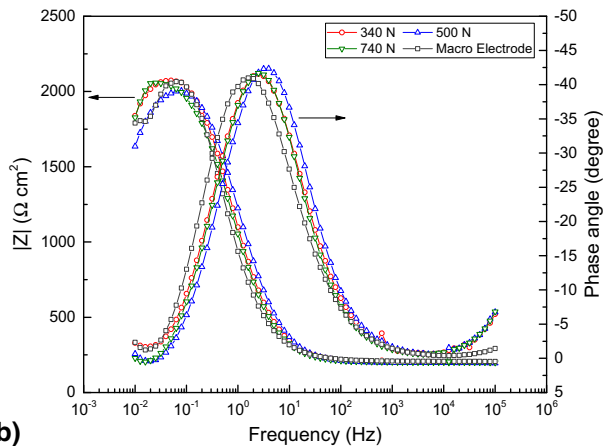
Fig. 5 Nyquist diagrams (a) and Bode plots (b) measured at the crack tip and on a macroscopic steel specimen under various applied loads in NS4 solution, respectively
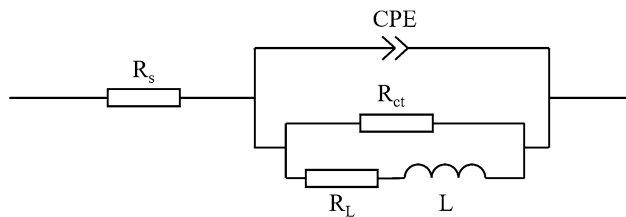

Fig. 6 Electrochemical equivalent circuit used to fit the measured impedance data

The measured impedance data were fitted with an equivalent circuit shown in Fig. 6, where R_s is solution resistance, R_{ct} is charge-transfer resistance, R_L is inductive resistance, L is inductance, and CPE is a constant phase element, which is used to simulate the double-layer capacitance of a steel electrode with inhomogeneous surface condition. The impedance of the CPE can be described as $Z_{CPE} = 1/CPE(j\omega)^n$, where ω is angular frequency, and n is a constant between 0 and 1. For a pure capacitor, n is equal to 1. The fitting electrochemical impedance parameters are shown in Table 2. It is seen that the charge-transfer resistance decreases with the increasing load. Since the charge-transfer resistance is inversely proportional to corrosion rate of the steel, the steel corrosion is increased by the increasing applied load.

Figure 7 shows the potentiodynamic polarization curves measured at the crack tip and on a macroscopic steel specimen under various applied loads in NS4 solution, respectively. It is seen that the steel at the crack tip shows an active dissolution behavior in the solution. The corrosion potential (E_{corr}) and corrosion current density (i_{corr}) are fitted by Tafel extrapolation, and the results are shown in Table 3. It is seen that there is no obvious effect of the applied load on corrosion potential. However, the corrosion current density increases with the load. The result is consistent with the EIS results.

3.4 SVET Mapping

Figure 8 shows the SVET current density maps measured at the area around the crack tip on the specimen under various applied loads in NS4 solution. It is seen that the current density shows maximum values ahead of the crack tip, indicating a high local electrochemical activity at the crack tip compared to adjacent areas. With the increase in the applied load, the maximum current density decreases. When the load is up to 740 N, negative current densities are recorded. This suggests that cathode areas are formed on the specimen, compared to the anode areas with positive current densities.

3.5 Characterization of Fracture Surface

Figure 9 shows the morphology of the side surface and the fracture surface of the steel specimens after tensile testing in air and the NS4 solution, respectively. Due to corrosion, the side surface of the specimen after soaking in NS4 solution is rougher (after the corrosion products are removed) than that tested in air. The fracture surfaces of the specimens tested in both air and the solution contain dimples, indicating the ductile feature of the fracture.

Table 2 Electrochemical impedance parameters fitted from the measured impedance data at the crack tip and a macroscopic specimen under various applied loads in NS4 solution

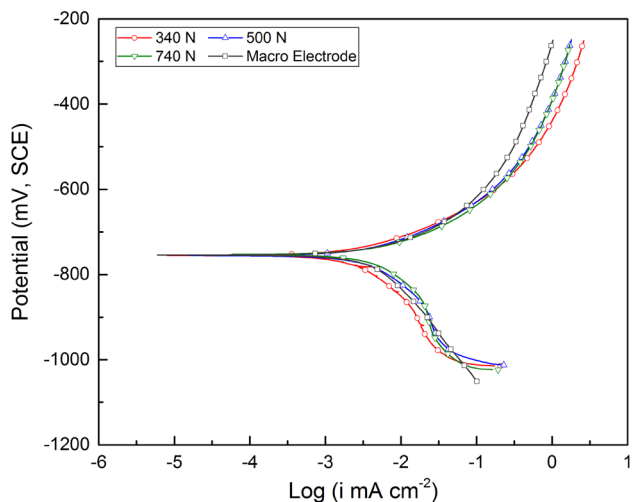| Load, N	R_s, Ω cm^2	R_{ct}, Ω cm^2	CPE, Ω^{-1} cm^{-2} s^{-n}	n	R_L, Ω cm^2	L, H cm^2
Macro-electrode (no applied load)	207	2300	2.65×10^{-4}	0.751	7617	23,702
340	201	2095	1.90×10^{-4}	0.775	17,247	51,485
500	197	1952	1.46×10^{-4}	0.800	13,176	54,363
740	201	1887	1.88×10^{-4}	0.799	12,182	111,290

Fig. 7 Potentiodynamic polarization curves measured at the crack tip and on a macroscopic steel specimen under various applied loads in NS4 solution, respectively

Table 3 Electrochemical parameters fitted from the measured polarization curves

Load, N	E_{corr}, mV, SCE	i_{corr}, μA/cm²
Macro-electrode (no applied load)	−754	3.85
340	−755	4.33
500	−755	4.52
740	−753	6.68

4. Discussion

4.1 Mechanistic Aspects of SCC of X46 Steel in Near-Neutral pH Solutions

It has been realized (Ref 1) that the near-neutral pH SCC of buried pipelines is associated with a diluted bicarbonate electrolyte having a pH between 5.5 and 7.5 trapped under the disbonded coating, polyethylene tape primarily. Carbon dioxide is typically generated from decay of organic matters and geochemical reactions in soils and becomes dissolved in the electrolyte to balance the pH. Near-neutral pH cracking of pipelines occurs under conditions where there is little, if any, cathodic protection (CP) current reaching the pipe surface over a prolonged service period, either because of the presence of a shielding coating, a highly resistive soil, or ineffective CP. Typically, the SCC colonies initiate at locations on the outside pipe surface where there is already pitting corrosion. The propagation of near-neutral pH stress corrosion cracks depends on the synergic effect of stress, hydrogen and anodic dissolution at the crack tip of the steel (Ref 1, 8, 9). It is generally accepted (Ref 20) that hydrogen accumulating at the crack tip increases the local embrittlement and enhances the cracking process. Meanwhile, the corrosion reaction occurring at the crack tip would accelerate the crack propagation (Ref 10, 11). The crack growth rate depends on three interrelated factors, i.e., stress-enhancing dissolution factor, hydrogen-enhancing dissolution factor and stress-hydrogen synergistic factor.

Generally, the SCC mechanism, which is either dominated by anodic dissolution (AD) or hydrogen embrittlement (HE), is determined by evaluating the potential of the steel (Ref 6). Figure 10 shows the potentiodynamic polarization curves measured on X46 steel in NS4 solution at scan rates of 0.5 and 100 mV/s, respectively. The low and high scan rates during polarization testing are used in order to simulate the electrochemical behavior on the crack wall and at the crack tip, respectively. It is seen that the curves are divided into three zones by the dashed lines, i.e., the two potentials at null current. Zone I is above potential of −755 mV (SCE). The SCC occurring in this zone is AD dominated as the steel is in an active dissolution state. Zone III is more negative than −928 mV (SCE), where the SCC mechanism is HE based. Zone II represents a potential range from −928 mV (SCE) to −755 mV (SCE), where the steel suffers from SCC by a mixed AD and HE mechanism. The corrosion potential of X46 steel at the crack tip in NS4 solution is about −755 mV (SCE), as shown in Fig. 7, suggesting that the SCC of the steel is dominated by the anodic dissolution mechanism, while the effect of hydrogen on the cracking is negligible. The ductile feature of the fracture surface obtained in NS4 solution, as seen in Fig. 9, also proves that the hydrogen-induced embrittlement does not occur on the steel under the present condition. The dissolution-based SCC behavior of the steel in NS4 solution causes the changes of mechanical properties and the ductility loss, as indicated in Table 1.

4.2 Effect of Stress on Anodic Dissolution at the Crack Tip

The corrosion current density at the crack tip increases with the increasing applied load, as shown in Table 3. The results indicate that the local anodic dissolution is enhanced by stress. Meanwhile, the EIS fitting results in Table 2 show the decrease in the charge-transfer resistance, i.e., the increase in the corrosion rate, at the crack tip with the applied load. Thus, the corrosion reaction at the crack tip is increased by the local stress and affects the crack propagation. The stress-enhanced corrosion effect was investigated by authors' previous work (Ref 21, 22). There are several millivolts of potential difference between a stress-free steel electrode and a stressed electrode, resulting in different electrochemical activities between them. The corrosion activity of the latter is higher than the former, depending on the stress level. This is primarily attributed to the resulting dislocation generation due to stressing of the steel.

During corrosion of pipeline steels in NS4 solution, a layer of porous corrosion products is formed on the steel surface, as shown in Fig. 11. Generally, the porous products provide somewhat protection to the steel from further corrosion (Ref 23). Thus, although an applied load (stress) enhances corrosion at the crack tip, the corrosion products could reduce the corrosion current density. As seen in Fig. 8, the maximum current density decreases when the applied load is increased from 340 to 500 N and 740 N. This is attributed to the deposit of corrosion products at the crack tip. It is noted that the local stress intensity factor, rather than applied load, is usually used as a basic parameter to define the stress status of a specimen. In this work, pre-cracked specimens were used, and numerical modeling was conducted to determine the stress at the crack tip on the specimen under various applied loads. Since the load is the directly controlled variable and the pre-crack is machined to follow the ASTM standard, it is thus used as the basic
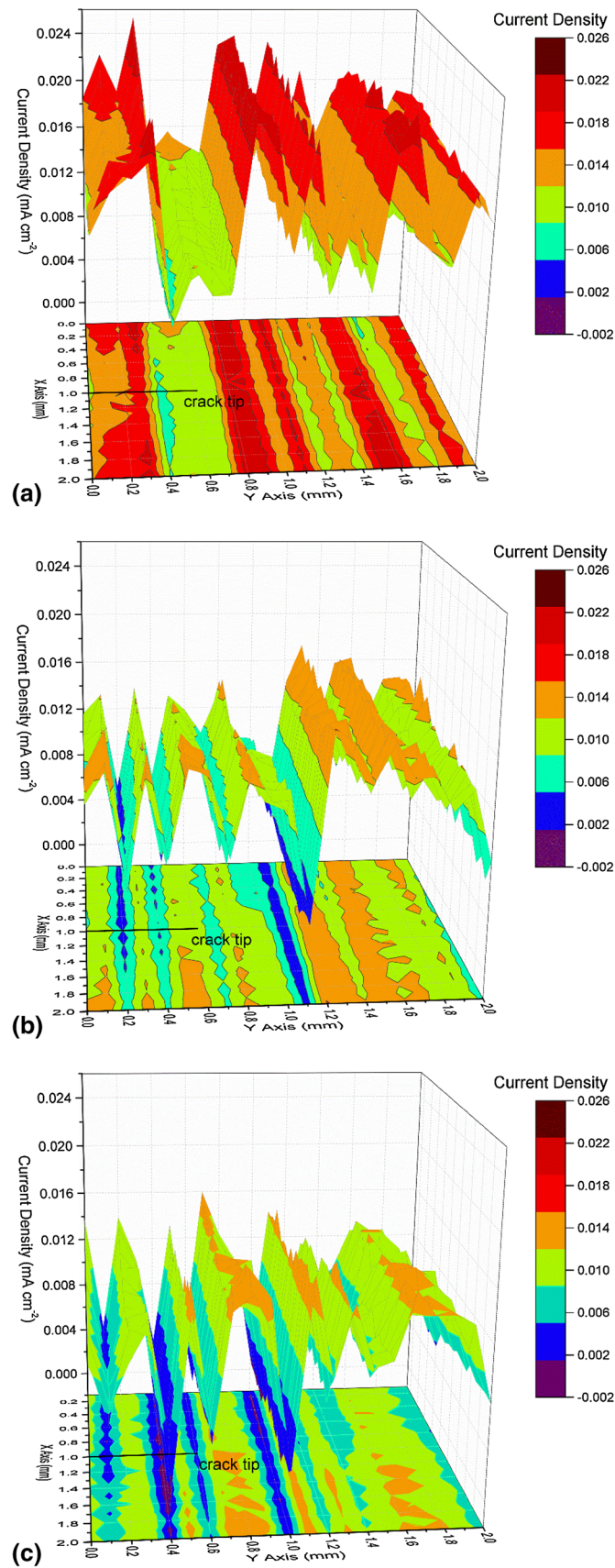
Fig. 8 SVET current density maps measured at the area around the crack tip on the specimen under various applied loads in NS4 solution (a) 340 N, (b) 500 N, and (c) 740 N, where the horizontal panels show the projected current density on the electrode surface
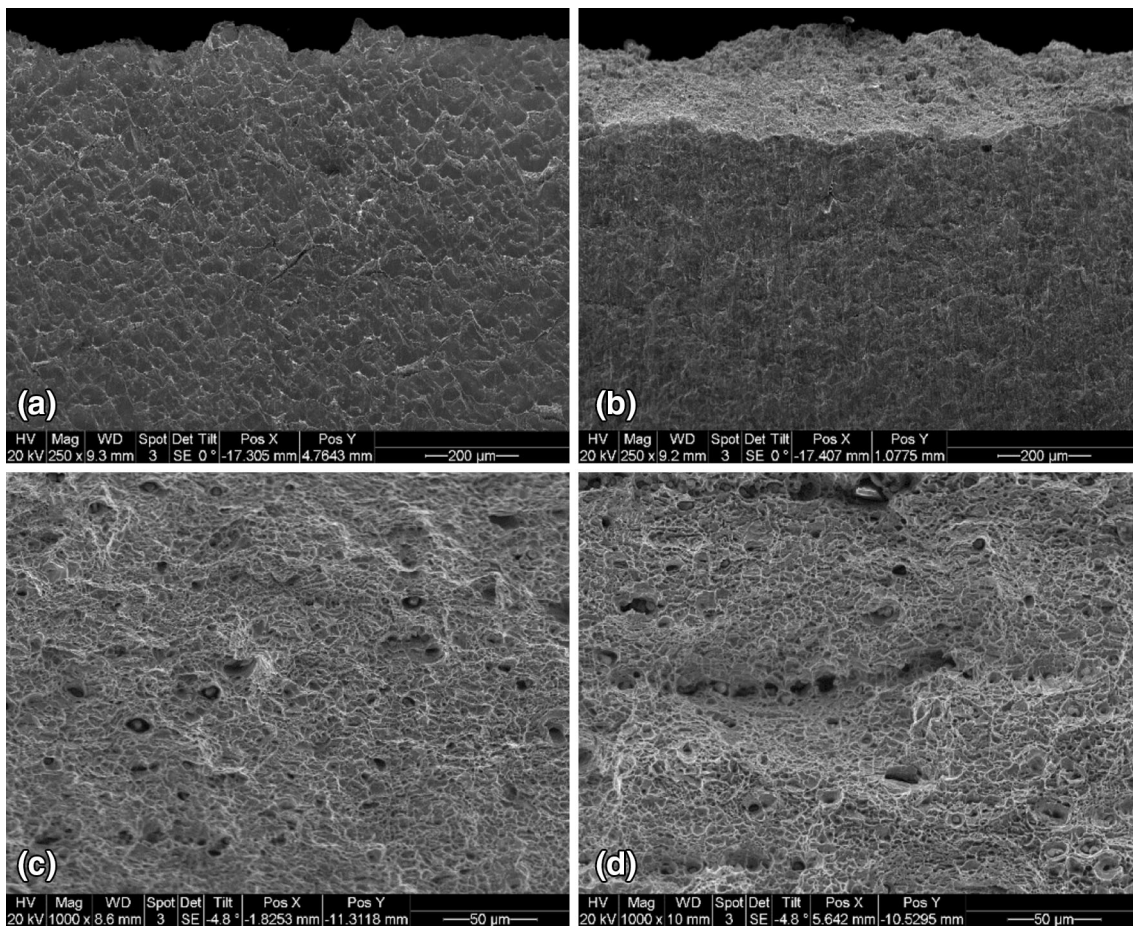
Fig. 9 SEM morphology of the side surface and the fracture surface of the steel specimens after tensile testing in air and the NS4 solution, respectively, (a) side, in air (b) side, in NS4 solution (c) fracture surface, in air (d) fracture surface, in NS4 solution
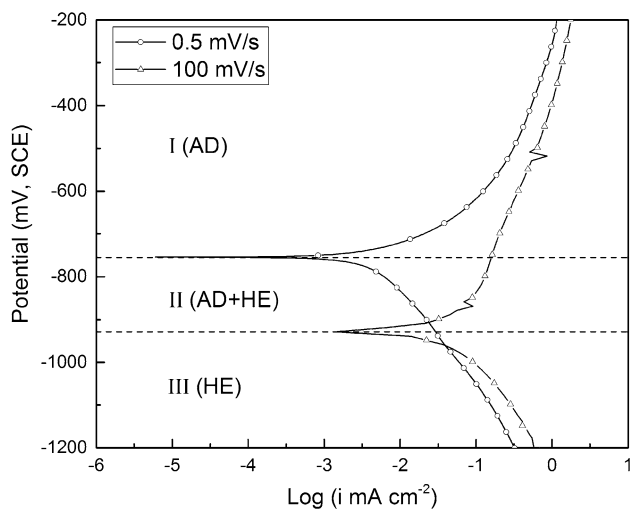

Fig. 10 Potentiodynamic polarization curves measured on X46 steel in NS4 solution at scan rates of 0.5 mV/s and 100 mV/s, respectively

Fig. 11 SEM view of corrosion products formed at the crack tip in NS4 solution

parameter. In other words, for the given pre-crack and testing conditions, the load is used for comparison.

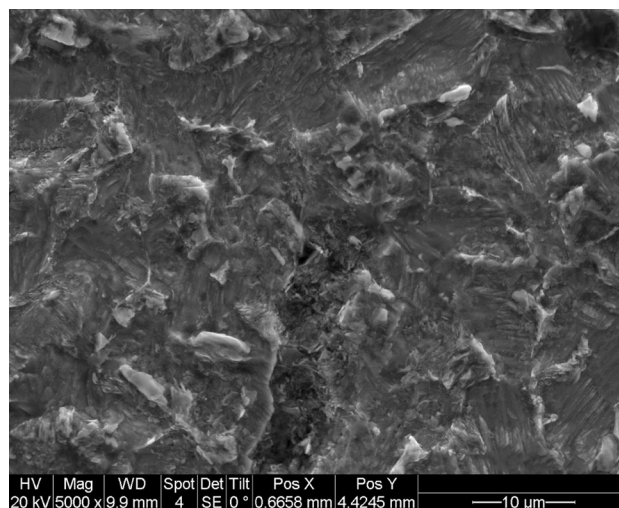As the layer of corrosion products thickens at sufficiently large applied loads, such as 740 N in this work, some areas become cathodic relative to the bare steel at the pores, which serve as the anode. The negative current recorded in SVET map in Fig. 8 demonstrates the presence of separated cathode and anode on the steel surface. This corrosion scenario could

contribute to initiation and propagation of corrosion pits and cracks.

5. Conclusions

The SCC of X46 pipeline steel in the near-neutral pH NS4 solution is dominated by the anodic dissolution mechanism, while the effect of hydrogen on the cracking is negligible. This is confirmed by the ductile feature of the fracture surface, and the potentiodynamic polarization measurements at both fast and slow potential scanning rates.

The applied load (stress) increases the corrosion rate of the steel at the crack tip, contributing to accelerated crack propagation.

The deposit of corrosion products at the crack tip could protect somewhat the steel from further corrosion, resulting in reducing local current density. At sufficiently large applied loads such as 740 N in the work, it is possible to generate separated cathode and anode on the corrosion product covered steel surface, further accelerating the crack growth.

References

1. Y.F. Cheng, *Stress Corrosion Cracking of Pipelines*, Wiley, Hoboken, 2013
2. National Energy Board, *Stress Corrosion Cracking on Canadian Oil and Gas Pipelines*, Calgary, AB, 1996
3. M. Javidi and S. Bahalaou, Horeh, Investigating the Mechanism of Stress Corrosion Cracking in Near-Neutral and High pH Environments for API, 5L X52 Steel, *Corros. Sci.*, 2014, **80**, p 213–220
4. X.Y. Zhang, S.B. Lambert, and R. Sutherby, Transgranular Stress Corrosion Cracking of X-60 Pipeline Steel in Simulated Ground Water, *Corrosion*, 1999, **55**, p 297–305
5. B.Y. Fang, E.H. Han, J.Q. Wang, and W. Ke, Stress Corrosion Cracking of X-70 Pipeline Steel in Near Neutral pH Solution Subjected to Constant Load and Cyclic Load Testing, *Corros. Eng., Sci. Technol.*, 2007, **42**, p 123–129
6. Z.Y. Liu, X.G. Li, and Y.F. Cheng, Mechanistic aspect of Near-Neutral pH Stress Corrosion Cracking of Pipelines under Cathodic Polarization, *Corros. Sci.*, 2012, **55**, p 54–60
7. G. Liang, X. Peng, E.S. Juan, and Y.F. Cheng, Strain Aging of X100 Steel in Service and the Enhanced Susceptibility of Pipelines to Stress Corrosion Cracking, *J. Mater. Eng. Perform.*, 2013, **22**, p 3778–3782
8. Y.F. Cheng, Analysis of Electrochemical Hydrogen Permeation Through X-65 Pipeline Steel and its Implications on Pipeline Stress Corrosion Cracking, *Int. J. Hydrog. Energy*, 2007, **32**, p 1269–1276
9. H.B. Xue and Y.F. Cheng, Hydrogen Permeation and Electrochemical Corrosion Behavior of X80 Pipeline Steel Weld, *J. Mater. Eng. Perform.*, 2013, **22**, p 170–175
10. G.A. Zhang and Y.F. Cheng, Micro-Electrochemical Characterization of Corrosion of Pre-Cracked X70 Pipeline Steel in a Concentrated Carbonate/Bicarbonate Solution, *Corros. Sci.*, 2010, **52**, p 960–968
11. X. Tang and Y.F. Cheng, Micro-Electrochemical Characterization of the Effect of Applied Stress on Local Anodic Dissolution Behavior of Pipeline Steel under Near-Neutral pH Condition, *Electrochim. Acta*, 2009, **54**, p 1499–1505
12. Y.F. Cheng, Fundamentals of Hydrogen Evolution Reaction and its Implications on Near-Neutral pH Stress Corrosion Cracking of Pipelines, *Electrochim. Acta*, 2007, **52**, p 2661–2667
13. A. Turnbull, The Solution Composition and Electrode Potential in Pits, Crevices and Crack, *Corros. Sci.*, 1983, **8**, p 833–870
14. I. Dmytrakh, Corrosion Fracture of Structural Metallic Materials: Effect of Electrochemical Conditions in Crack, *Strain Int. J. Exp. Mech.*, 2011, **47**, p 427–435
15. Z.Y. Liu, X.G. Li, and Y.F. Cheng, Effect of Strain Rate on Cathodic Reaction During Stress Corrosion Cracking of X70 Steel in a Near-Neutral pH Solution, *J. Mater. Eng. Perform.*, 2011, **20**, p 1242–1246
16. ASTM, E647-15, Standard Test Method for Measurement of Fatigue Crack Growth Rates, West Conshohocken, PA, USA, 2015
17. R.N. Parkins, W.K. Blanchard, and B.S. Delanty, Transgranular Stress Corrosion Cracking of High-Pressure Pipelines in Contact with Solutions of Near Neutral pH, *Corrosion*, 1994, **50**, p 394–408
18. ASTM, E8/E8M Standard Test Methods for Tension Testing of Metallic Materials, West Conshohocken, PA, USA, 2010
19. ASTM G59-97, Standard Test Method for Conducting Potentiodynamic Polarization Resistance Measurements, West Conshohocken, PA, USA, 2014
20. C.F. Dong, Z.Y. Liu, X.G. Li, and Y.F. Cheng, Effects of Hydrogen-Charging on the Susceptibility of X100 Pipeline Steel to Hydrogen-Induced Cracking, *Int. J. Hydrog. Energy*, 2009, **34**, p 9879–9884
21. L.Y. Xu and Y.F. Cheng, Corrosion of X100 Pipeline Steel under Plastic Strain in a Neutral pH Bicarbonate Solution, *Corros. Sci.*, 2012, **64**, p 145–152
22. L.Y. Xu and Y.F. Cheng, An Experimental Investigation of Corrosion of X100 Pipeline Steel under Uniaxial Elastic Stress in a Near-Neutral pH Solution, *Corros. Sci.*, 2012, **59**, p 103–109
23. G.Z. Meng, C. Zhang, and Y.F. Cheng, Effects of Corrosion Product Deposit on the Subsequent Cathodic and Anodic Reactions of X-70 Steel in Near-Neutral pH Solution, *Corros. Sci.*, 2008, **50**, p 3116–3122